Angewandte Chemie
Eine Zeitschrift der Gesellschaft Deutscher Chemiker

Supporting Information

A Rapidly Responsive Sensor for Wireless Detection of Early and Mature Microbial Biofilms

A. Shafaat, J. F. Gonzalez-Martinez, W. O. Silva, A. Lesch, B. Nagar, Z. Lopes da Silva, J. Neilands, J. Sotres, S. Björklund, H. Girault, T. Ruzgas**

Supporting Information

Table of contents:

S1. Materials and methods

S1.1. Materials

Phosphate-buffered saline (PBS) tablets, formaldehyde solution 4% (buffered, pH 6.9), Human serum, hexamethyldisilazane (HMDS) and silver dispersion (nanoparticle, 30-35 wt.% in triethylene glycol monomethyl ether) were purchased from Sigma-Aldrich. All aqueous solutions were prepared in ultrapure water (resistivity of 18.2 MΩ cm) purified by a Purelab Flex system (ELGA LabWater, High Wycombe, UK). A woven carbon cloth without a microporous layer (thickness of 330 µm and through plane electrical resistivity of < 5 mΩcm²) was purchased from Fuel Cell Store (Texas, USA) and was used as the anode for hosting the growth of microorganisms.

S1.2. Inkjet printing combined with flashlight sintering (FLS)

The printing process shown in Figure S1A was carried out by using a DMP-2831 Dimatix Fujifilm inkjet printer and a DMC11610 Dimatix Fujifilm disposable cartridge containing 16 individual nozzles of 10 pL nominal droplet volume. Firstly (step 1), two legs and one bridge/connection were printed on a thermostabilized polyethylene terephthalate (PET) substrate (Folex®, thickness 180 µm) using a commercial silver ink (nanoparticle, 30-35 wt.% in triethylene glycol monomethyl ether). During the printing process the PET substrate was heated at 60 °C in order to promote solvent evaporation and improve the printing resolution. Secondly (step 2), the dried silver film was sintered by flashlight irradiation using a Xenon flash lamp (PulseForge 1300 photonic curing system, Novacentrix, USA). This non-equilibrium thermal method promotes the heating of the printed, light-absorbing Ag film to several hundred degrees centigrade (Fig. S1B and C) in a very short time (10.5 ms) while the weak light-absorbing PET remained cold. Here, the advantage compared to the conventional thermal sintering method is not only the short heating time but also that the fast process does not damage the PET substrate. The flashlight sintering (FLS) was performed with a 10.5 ms 420 V-pulse; one flash shot corresponded to 13 micro pulses with a total energy density of 3.4 $J \cdot cm^{-2}$ as illustrated in Figure S1B. Complete silver sintering was achieved using 5 consecutive flash shots during a total time of 12.2 s as presented in Figure S1C; additional details of the FLS process can be found in previous works [1]. Thirdly (step 3), a colorless and UV-curable dielectric ink (Bectron® IJ 5001 VP Insulating ink, Elantas) was printed and then (step 4) photopolymerized by a UV lamp during 5 s (FireFly 25x10, 395 nm, 4 W/cm^2, Phoseon Technology) in order to generate a dielectric layer and thus isolating the conductive legs and also to precisely define the exposed silver bridge area that was used as the cathode segment.

S1.3. Microorganism strains and growth conditions

The microorganism model selected in this work was the co-culture of *Pseudomonas aeruginosa* (PA01) and *Staphylococcus aureus* (ATCC29213) obtained from the Department of Oral Biology (Faculty of Odontology, Malmö University). Each type of bacteria was grown separately on blood agar in 5% carbon dioxide (CO_2) at 37 °C. In order to get the stationary phase, the colonies were transferred into liquid Luria–Bertani (LB) medium (10 g L^{-1} tryptone, 5 g L^{-1} yeast extract and 10 g L^{-1} sodium chloride, pH 7.3 ± 0.2) and incubated at 37 °C for 18 hours with shaking at 200 rpm. To get the final concentration of 10^7 CFU/mL, the optical density at 600 nm was adjusted to be about 0.066 for *P. aeruginosa* and 0.16 for *S. aureus*. Following that, a mixture containing 5 mL of *S. aureus* and 500 µL of *P. aeruginosa* was diluted with LB medium in a total volume of 50 mL, where the concentration of *P. aeruginosa* in the co-culture was 10 times less than that of *S. aureus* (10^6:10^5 CFU/mL) to avoid its predominance after cultivation. In spite of the synergistic interaction between the two species in biofilm formation, in planktonic co-cultures, *P. aeruginosa* outcompetes *S. aureus* and becomes the dominant species. This has been attributed to some products of *P. aeruginosa* including 2-n-heptyl-4-hydroxyquinoline-N-oxide (HQNO) that affects the electron transport chain of *S. aureus*, alters the essential genes to non-essential type and inhibits the oxidative respiration [2]. To avoid this and for their better coexistence, the ratio of 10:1 (*S. aureus*: *P. aeruginosa*) has been selected in this work according to the previously reported *in vivo* and *in vitro* wound models [3]. To investigate the microbial biofilm growth in close to authentic conditions, the measurements were

performed in simulated wound fluid prepared by mixing 50% of Human serum and 50% of peptone water (0.9% NaCl in 0.1% peptone).

S1.4. Scanning Electron Microscopy (SEM) and Confocal Laser Scanning Microscopy (CLSM)

To analyze the biofilm formed on carbon cloth by microscopy techniques, the substrates were placed in the co-culture of *S. aureus* with *P. aeruginosa* (10:1) and the microorganisms were grown at 37 °C for different time points, ranging from 30 min to 24 h. For scanning electron microscopy, 5×5 mm^2 pieces of the carbon cloth taken from different time points were first incubated/fixed in a solution of 4% formaldehyde (buffered, pH 6.9) for 5 min. The samples were then washed in deionized water for 10 min. Dehydration of the samples was performed using ethanol 30, 50, 70, 90, and 100 (vol %), 10 min in each solution. Following this step, the samples were immersed in hexamethyldisilazane (HMDS) for 15 min and then left to dry at room temperature to be ready for the SEM analysis. For confocal laser scanning microscopy, the 5×5 mm^2 pieces of carbon cloth taken from different time points were assessed after staining with the Live/Dead BacLight staining kit (Life Technologies, Stockholm, Sweden).

S1.5. OCP measurements

Open circuit potential (OCP) measurements in both fresh LB medium (as control) and co-culture of *S. aureus* with *P. aeruginosa* (10:1) were performed using a Multichannel Potentiostat/Galvanostat µStat 8000. Microorganisms were grown for 24 h (at 37 °C) while the OCP was recording continuously between the carbon cloth and a double junction Ag/AgCl (3 M KCl (gel-based)) reference electrode.

S1.6. Current measurements

Measurements of the current generated by the biofilm were performed using a Multichannel Potentiostat/Galvanostat µStat 8000 in the co-culture of *S. aureus* with *P. aeruginosa* (10:1), as well as individually in monocultures. The measurements were conducted with the polarization potential of 0 mV for 24 h (at 37 °C) in a three-electrode system comprising carbon cloth, a carbon rod, and a double junction Ag/AgCl (3 M KCl (gel-based)) as working, counter, and reference electrodes, respectively.

S1.7. Cyclic voltammetry (CV), linear sweep voltammetry (LSV) and chronopotentiometry measurements

In order to characterize the amounts of printed Ag in different batches of inkjet printed electrodes (IJPE), cyclic voltammograms were recorded in PBS in the potential range of -0.3 to 0.3 V (vs. SCE) with a scan rate of 10 mV s^{-1} and step potential of 1 mV. The measurements were performed using an Ivium potentiostat (CompactStat) in a three-electrode system where a platinum wire and a saturated calomel electrode (SCE) were used as auxiliary and reference electrodes, respectively. The amounts of exposed printed Ag, constituting the sensing bridge cathode, were then calculated using the obtained cyclic voltammogram. This was done by first converting the corresponding voltammogram (i vs. E) to the plot of current vs. time (considering scan rate and step potential values) and then integrating the area under the curve according to $Q = \int_{t_1}^{t_2} i(t)\, dt$.

To estimate the time needed for the reduction of AgCl to Ag (*i.e.*, the sensor response time), simple experiments were performed using linear sweep voltammetry (LSV) following chronopotentiometry. Accordingly, linear sweep voltammograms were recorded in the potential range of -0.3 to 0.3 V (vs. SCE) with a scan rate of 10 mV s^{-1} and step potential of 1 mV to convert printed Ag to AgCl in PBS solution. Following this step, -2µA was applied in chronopotentiometry mode. At the -2µA constant current, AgCl was reduced to Ag. The amounts of Ag in LSV measurements were calculated in the same way as performed in cyclic voltammetry. In chronopotentiometry mode, however, the amount of charge was calculated using the time needed for the reduction of AgCl multiplied by a constant current of -2µA ($Q = it$).

S1.8. Measurements of the bioanode driven reduction of AgCl to Ag on the cathode

To measure the bioanode driven reduction of AgCl, first, the exposed area of the silver inkjet printed electrode was electrochemically oxidized to AgCl using an applied potential of 200 mV (vs. SCE) for 120 s in PBS. Following this step, the carbon cloth, with adhered grown biofilm, was connected to the inkjet printed electrode hosting two electrodes bridged by an electrochemically oxidized AgCl layer. The described set-up was immersed in LB medium and the current flow between two electrodes of the inkjet printed electrode, across the AgCl bridge, was measured by a potentiostat in chronoamperometric mode with 5 mV applied DC voltage. The current measurements were then used to calculate the resistance of the transduction layer using Ohm´s law.

S1.9. Measurement of the solution resistance (R_2), by electrochemical impedance spectroscopy (EIS)

In order to obtain the resistance of the solutions prepared for modelling of the equivalent circuit (called R_2), electrochemical impedance spectroscopy (EIS) was conducted on AgCl/IJPE in buffer solutions with different ionic strength at an AC voltage amplitude of 10 mV, DC applied potential of 0.0 V and a frequency range of 10 MHz to 0.1 Hz.

S1.10. Wireless measurement of AgCl to Ag conversion: recording of $|S_{11}|$ characteristic

To analyze the impedance of the tag antenna, a Vector Network Analyzer DG8-SAQ, VNA (SDR-Kits, Melksham, UK) was used as a wireless reader. The reader antenna was made of copper in circular shape (diameter 4 cm, 4 loops) connected to the TX port of the vector network analyzer. A near-field communication (NFC) tag (Smartrac, operating frequency 13.56 MHz) was used as the biosensor RF antenna, enabling the wireless detection of biofilm formation. 5 mm of this antenna was then cut out for connecting to the AgCl/IJPE cathode and the carbon cloth bioanode as shown in Figure S2. The magnitude of the reflection parameter $|S_{11}|$ was monitored continuously in the frequency range of 3-32 MHz while the distance between the reader and the tag antennas was kept constant at 1 cm. The magnitude of $|S_{11}|$ is defined by the following relation:

$$|S_{11}| = \sqrt{1 - \frac{P_T(f)}{P_{MAX}(f)}}$$

Where, P_T is the transmitted power to the tag antenna at a certain frequency and P_{MAX} is the maximum achievable transmitted power.

S2. Inkjet printing and flashlight sintering of the silver transduction layer

In this work, the cathode part is made by inkjet printing of silver ink on the surface of flexible PET cured by FLS. Figure S1A shows the required steps for manufacturing the cathode layer. These include (*i*) printing of the silver legs and bridge (*ii*) photonic curing of silver using a Xenon lamp to form a conductive path, (*iii*) covering with a UV-curable insulation layer followed by *(iv)* photopolymerization. The UV-curable ink insulates the silver conductive legs and a part of the bridge in order to define a specific silver area exposed to the electrolyte. The exposed Ag layer will be then oxidized electrochemically in PBS to AgCl and placed as a part of the tag antenna for further wireless measurements.

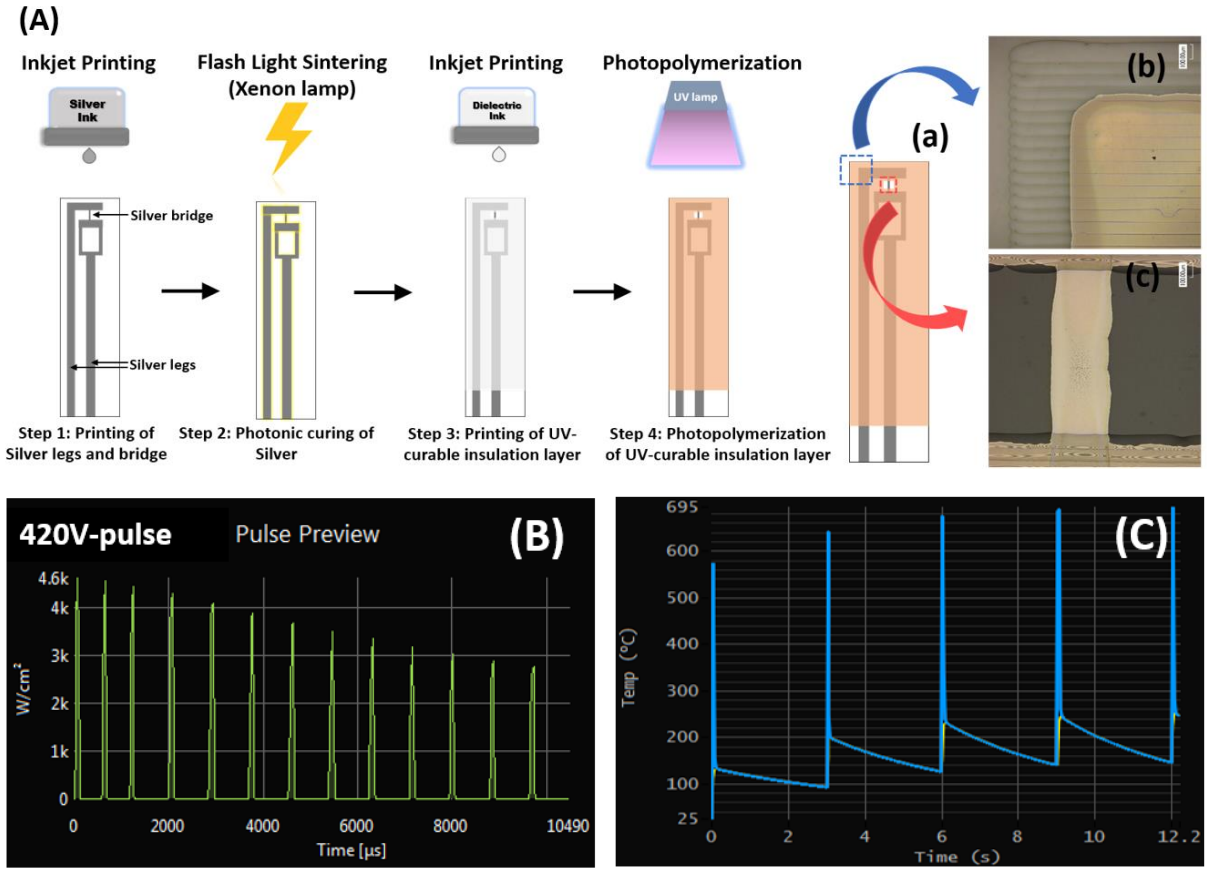

Fig. S1. (A) Manufacturing steps of the transduction layer with two electrodes short-circuited by one silver layer/bridge generated by inkjet printing and flashlight sintering. (a-c) Photopolymerized UV-curable dielectric film and dried silver bridge printed on PET substrate. **(B)** Flashlight irradiation profile of one apparent flash shot containing 13 micro pulses generated at 420 V-pulse during 10.5 ms. **(C)** simulated temperature profile obtained on the silver film during 5 flash shots.

S3. Characteristics of the proposed setup for wireless measurement of early and mature biofilm

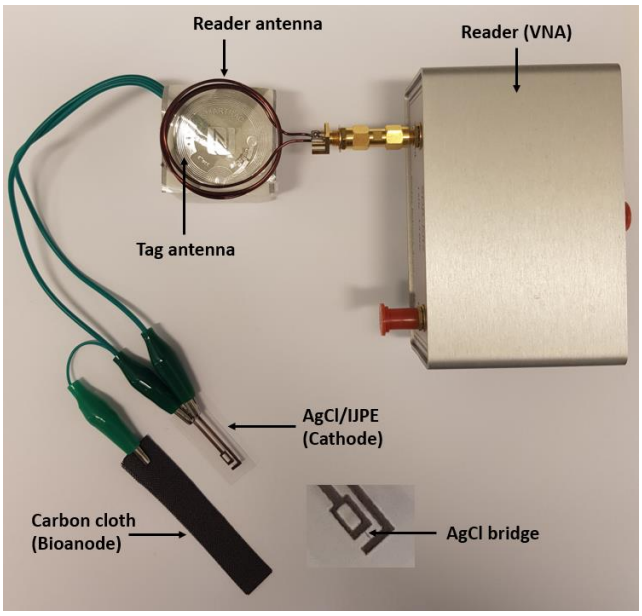

Fig. S2. A photograph of the setup including the reader (Vector Network Analyzer, VNA) equipped with a homemade copper antenna and NFC tag with 5 mm cut out of antenna for connecting to the AgCl/IJPE cathode and the carbon cloth bioanode.

S4. Open circuit potential (OCP) measurement of carbon cloth in LB medium

As the negative control, the open circuit potential (OCP) of the carbon cloth was recorded continuously in LB medium (without microorganisms) at 37 °C versus a double junction Ag/AgCl (3 M KCl (gel-based)) reference electrode (Fig. S3). Compared to the results in the presence of the co-culture of *S. aureus* and *P. aeruginosa* (shown in Fig. 2A, main text), the potential starts from the initial values of 78 mV±6.2, decreases almost 12 mV in the first hour and remains constant at positive values for the rest of the measurement confirming that the negative potential can be obtained in the presence of bacteria only.

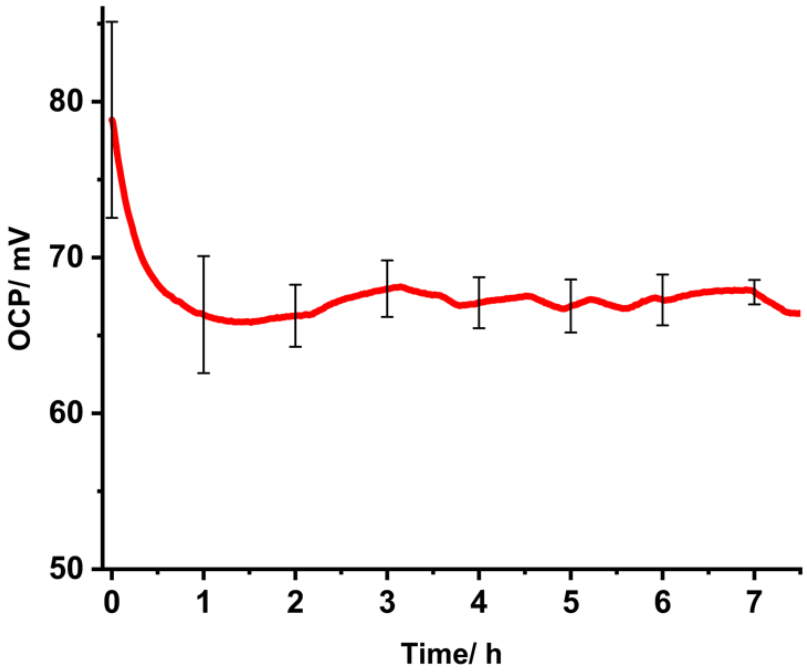

Fig. S3. Open circuit potential (OCP) of the carbon cloth in LB medium recorded continuously versus a double junction Ag/AgCl (3 M KCl (gel-based)) reference electrode. The error bars represent the standard deviation of measured data for three independent experiments.

S5. Optimization of the printing properties to determine the Ag/AgCl area exposed to the solution

The area (amount) of the silver exposed to the solution is one of the main features of the transduction layer. In general, higher amounts of AgCl exposed to the electrolyte require a longer time to be reduced to Ag (for the same amount of current). In this work, the bridge of silver with a length of ~1 mm and three different widths, 0.05, 0.1, and 0.2 mm was printed on the PET substrate, thus connecting the two Ag legs (Fig. S4A). The conductive legs and a part of the bridge (from two sides) were then covered with the insulation layer (Fig. S4B) to define the silver exposed areas, presented in Table S1. The amounts of printed Ag for different exposed areas were calculated by integrating the area under the cyclic voltammogram traces (Fig. S4C). As shown in Table S1, the smaller the area, the lower the amount of AgCl (*i.e.*, the charge Q) present in the cathode layer and as a result, a shorter time is required for reduction to Ag. However, according to the results provided in the same Table, decreasing the exposed surface area increases the resistance of the transduction layer. To keep a balance between loaded Ag (Q) and the resistance of the transduction layer (R), an area of 0.2mm× 0.37mm was selected as the optimized area exposed to the solution.

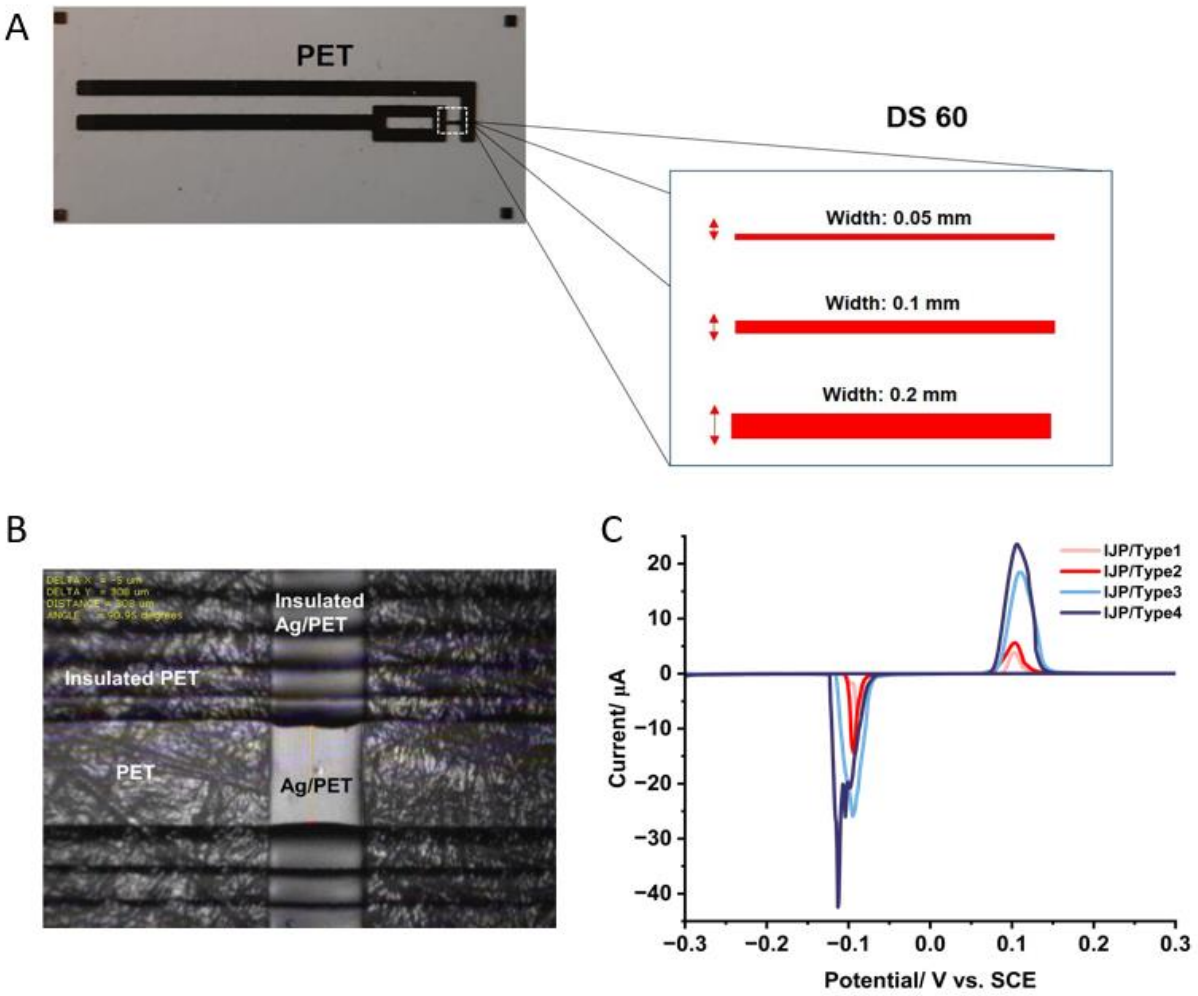

Fig. S4. (A) Photograph of inkjet printed silver electrode with a bridge length of ~1 mm and three different widths, 0.05, 0.1, and 0.2 mm, printed on PET substrate connecting two Ag legs. **(B)** After coverage with the insulation layer, the printed silver bridge defines the specific surface area exposed to the electrolyte. **(C)** Cyclic voltammograms were conducted in PBS for inkjet printed electrodes with different exposed areas specified in Table 1.

Table S1. Calculated charge (Q) using cyclic voltammetry and resistance (R) for silver inkjet printed electrodes with four different areas exposed to the electrolyte.

	The area exposed to the solution	**Q (µC)**	**R (Ω)**
IJP/Type1	DS60- W 0.05mm- L 0.38mm	11±2.5	98±17
IJP/Type2	DS60- W 0.1mm- L 0.21mm	14±2.3	80±5.2
IJP/Type3	DS60- W 0.2mm- L 0.37mm	65±3.5	66±6.1
IJP/Type4	DS60- W 0.2mm- L 0.43mm	82±4.4	58±3.4

S6. Characterization of the inkjet printed electrodes (IJPE) using electrochemical methods

More electrochemical measurements were performed on inkjet printed electrodes in order to investigate the possibility for estimation of sensor response time while detecting biofilm formation. The experiment simulates the conditions where the bridged AgCl in the cathode layer will be reduced using the current generated by the biofilm. Accordingly, the printed Ag layer was oxidized to AgCl using linear sweep voltammetry (Fig. S5A) and the amounts of deposited Ag were determined by integrating ($Q = \int_{t_1}^{t_2} i(t)\, dt$) the area under the corresponding current-time curve (Fig. S5B). The AgCl layer was subsequently reduced in chronopotentiometric mode by applying a current equivalent to that produced by bacterial activity in different stages of biofilm formation. Here, a current of -2 µA, a level comparable to the early stages of biofilm formation, was selected as the constant current to run chronopotentiometry and reduce AgCl to Ag (Fig. S5C). The charges calculated from linear sweep voltammetry were then plotted versus reduction times found in chronopotentiometry for different inkjet printed electrodes. The slope of 1.97 shown in Figure S5D is almost equivalent to the applied current of 2 µA and this confirms the linear relationship between charge and time, *i.e.*, the higher the charge, the longer the response time (for the same amount of current developed in the system). In the same way, for inkjet printed electrodes with a similar amount of AgCl (Q), the higher the current, the shorter time is required to get the same amount of charge (electrons) for the conversion of AgCl to Ag. According to the results shown in Figure 2B (main text), the current generated during the biofilm development shows an increase from the initial steps to the maturation levels, which corresponded to an increase of charge from 0.05 C to 2.73 C. Hence, for a given thickness of the AgCl layer, we expect a shorter response time detecting the matured biofilm compared to the detection of bacteria in the early stages.

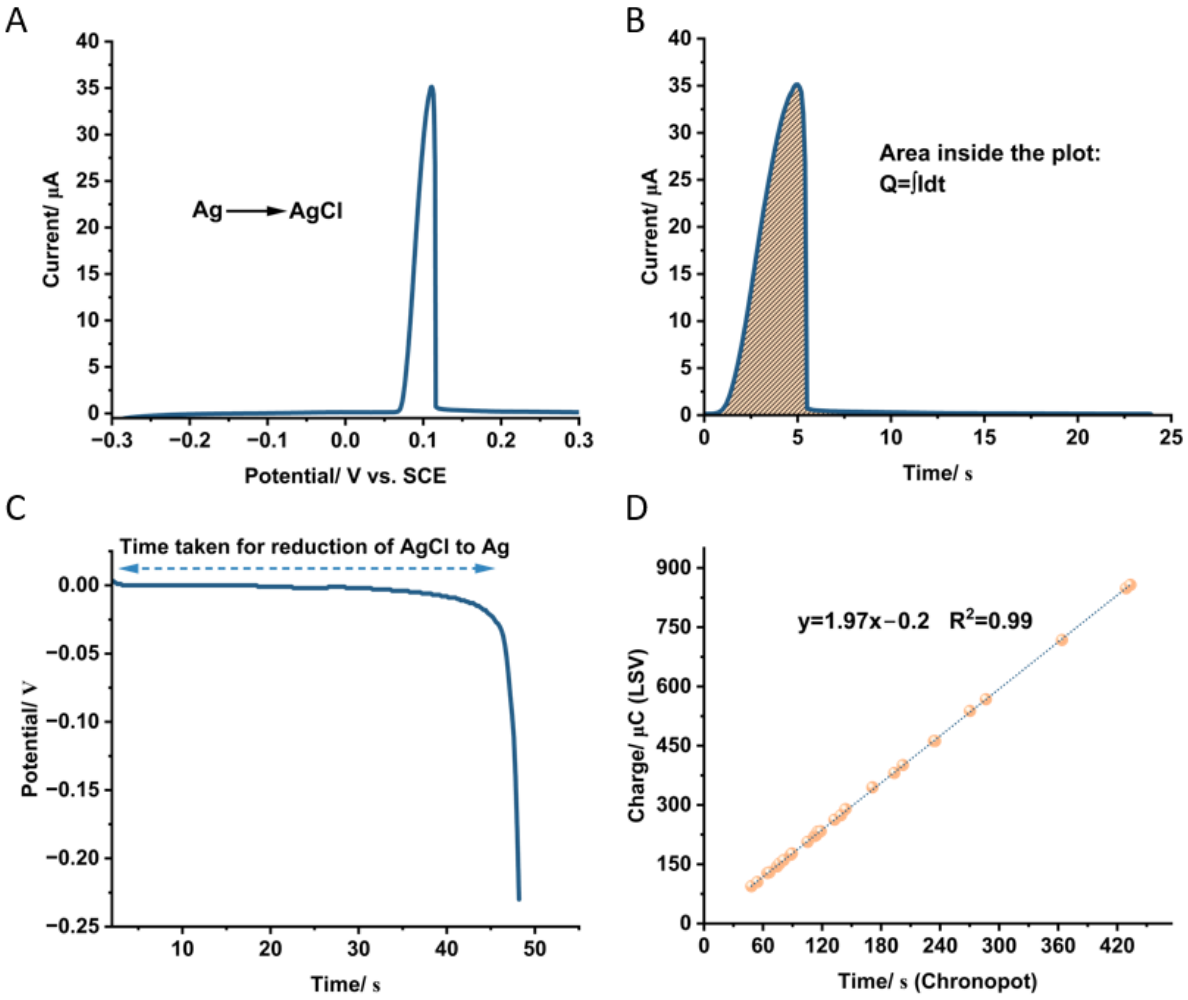

Fig. S5. (A) linear sweep voltammogram showing the oxidation of the printed Ag bridge to AgCl. **(B)** Equivalent i-t curve for the linear sweep voltammogram obtained in (A) which is used to calculate the electrical charge. **(C)** Chronopotentiometry at a constant current of -2µA for reduction of AgCl to Ag. **(D)** The charge plot calculated from linear sweep voltammetry versus time found in chronopotentiometry for different inkjet printed electrodes shows the linear relation between charge and time.

S7. Wireless monitoring of the growth of biofilm in the early stages in simulated wound fluid

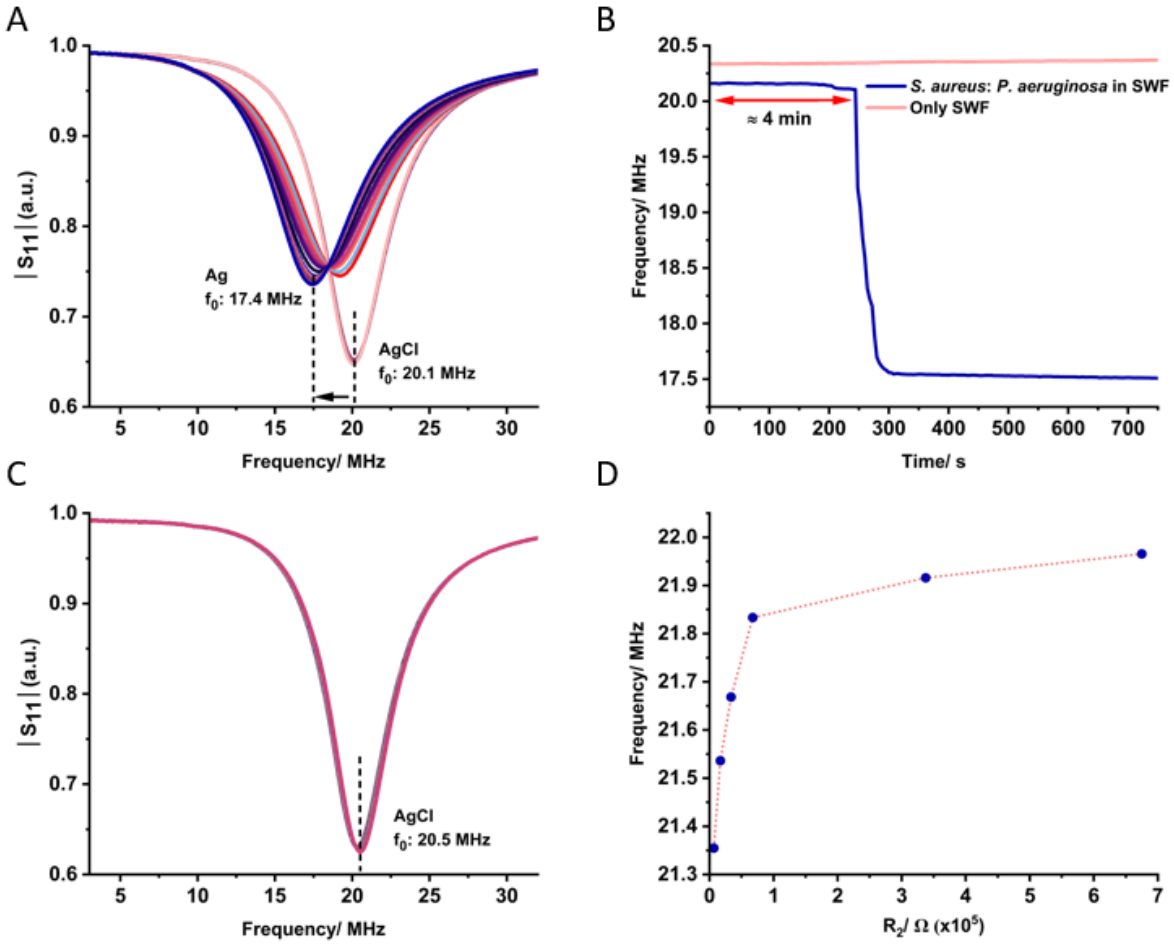

Fig. S6. (A) $|S_{11}|$ vs. frequency recorded in a setup similar to scheme 1, in which AgCl/IJPE as a part of tag antenna is in connection with the carbon cloth and both are immersed in the co-culture of *S. aureus* and *P. aeruginosa* (10:1) dispersed in simulated wound fluid (SWF). **(B)** Changes of the characteristic frequency of the wireless biosensor with AgCl/IJPE as a part of the tag antenna connected to the carbon cloth in response to the absence and presence of the co-culture of *S. aureus* and *P. aeruginosa* (10:1) dispersed in SWF. **(C)** $|S_{11}|$ vs. frequency recorded for 12 h in a setup similar to scheme 1, in which AgCl/IJPE as a part of tag antenna is in connection with the bare carbon cloth (no adhered planktonic bacteria or biofilm) immersed in SWF without any dispersed bacteria. **(D)** Dependency of the characteristic frequency of the tag antenna with a coupled AgCl/IJPE on the resistance of the solution (R_2).

S8. Description of the equivalent electrical circuit of the chip-less, wireless biosensor

Table S2. Values of R_2 obtained for AgCl/IJPE and the characteristic frequency f_0 measured for both Ag and AgCl/IJPE immersed in air, water, and buffer solutions with different ionic strength.

		Material of transduction layer		
		AgCl		**Ag**
Media where the IJPE with transduction layer is exposed to	I, mM	$f_{0(AgCl)}$, MHz	R_2, Ω (x10^5)	$f_{0(Ag)}$, MHz
Air	-	22.24612		17.21111
Pure water	-	21.89945	-	17.29365
PBS 100 times diluted	1.657	21.96548	6.75	17.22761
PBS 50 times diluted	3.314	21.91596	3.375	17.24412
PBS 10 times diluted	16.57	21.83342	0.675	17.21111
PBS 5 times diluted	33.14	21.66833	0.3375	17.1946
PBS 2.5 times diluted	66.28	21.53627	0.16875	17.11206
PBS	165.7	21.35468	0.0675	17.21111

References

[1] a) A. Bananezhad, M. Jović, L. F. Villalobos, K. V. Agrawal, M. R. Ganjali, H. H. Girault, *Journal of Electroanalytical Chemistry* **2019**, *847*, 113241; b) M. Jović, Y. Zhu, A. Lesch, A. Bondarenko, F. Cortés-Salazar, F. Gumy, H. H. Girault, *Journal of Electroanalytical Chemistry* **2017**, *786*, 69-76; c) B. Nagar, M. Jović, V. C. Bassetto, Y. Zhu, H. Pick, P. Gómez-Romero, A. Merkoçi, H. H. Girault, A. Lesch, *ChemElectroChem* **2020**, *7*, 460-468; d) B. Nagar, W. O. Silva, H. H. Girault, *ChemElectroChem* **2021**, *8*, 3700-3706.

[2] a) D. B. Y. Yung, K. J. Sircombe, D. Pletzer, *Molecular Microbiology* **2021**, *116*, 1-15; b) S. DeLeon, A. Clinton, H. Fowler, J. Everett, A. R. Horswill, K. P. Rumbaugh, *Infect Immun* **2014**, *82*, 4718-4728; c) Z. A. Machan, T. L. Pitt, W. White, D. Watson, G. W. Taylor, P. J. Cole, R. Wilson, *J Med Microbiol* **1991**, *34*, 213-217; d) P. M. Alves, E. Al-Badi, C. Withycombe, P. M. Jones, K. J. Purdy, S. E. Maddocks, *Pathogens and Disease* **2018**, *76*; e) P. W. Woods, Z. M. Haynes, E. G. Mina, C. N. H. Marques, *Frontiers in Microbiology* **2019**, *9*.

[3] a) C. B. Ibberson, A. Stacy, D. Fleming, J. L. Dees, K. Rumbaugh, M. S. Gilmore, M. Whiteley, *Nature Microbiology* **2017**, *2*, 17079; b) N. Yang, Q. Cao, S. Hu, C. Xu, K. Fan, F. Chen, C.-G. Yang, H. Liang, M. Wu, T. Bae, L. Lan, *Molecular Microbiology* **2020**, *114*, 423-442.